IEEE Access
Multidisciplinary | Rapid Review | Open Access Journal

IEEE MAGNETICS SOCIETY SECTION

Received May 27, 2021, accepted July 9, 2021, date of publication July 12, 2021, date of current version July 20, 2021.

Digital Object Identifier 10.1109/ACCESS.2021.3096740

Nanoflowers Versus Magnetosomes: Comparison Between Two Promising Candidates for Magnetic Hyperthermia Therapy

ELIZABETH M. JEFREMOVAS[1], LUCÍA GANDARIAS[2], IRATI RODRIGO[3], LOURDES MARCANO[3,4], CORDULA GRÜTTNER[5], JOSÉ ÁNGEL GARCÍA[6], ENEKO GARAYO[7], (Member, IEEE), IÑAKI ORUE[8], ANA GARCÍA-PRIETO[9], ALICIA MUELA[2], MARÍA LUISA FERNÁNDEZ-GUBIEDA[3], JAVIER ALONSO[1], AND LUIS FERNÁNDEZ BARQUÍN[1], (Member, IEEE)

[1]Departamento CITIMAC, Facultad de Ciencias, Universidad de Cantabria, 39005 Santander, Spain
[2]Departamento Inmunología, Microbiología y Parasitología, Universidad del País Vasco (UPV/EHU), 48940 Leioa, Spain
[3]Departamento de Electricidad y Electrónica, Universidad del País Vasco (UPV/EHU), 48940 Leioa, Spain
[4]Helmholtz-Zentrum Berlin für Materialien und Energie, 12489 Berlin, Germany
[5]Micromod Partikeltechnologie GmbH, 18119 Rostock, Germany
[6]Departamento de Física, Universidad del País Vasco (UPV/EHU), 48940 Leioa, Spain
[7]Departamento de Física Aplicada, Universidad Pública de Navarra, 31006 Pamplona, Spain
[8]SGIker Medidas Magnéticas, Universidad del País Vasco (UPV/EHU), 48940 Leioa, Spain
[9]Departamento de Física Aplicada I, Escuela de Ingeniería de Bilbao, 48013 Bilbao, Spain

Corresponding author: Elizabeth M. Jefremovas (martinjel@unican.es)

This work was supported in part by the Spanish "Ministerio de Ciencia, Investigación y Universidades" under Project MAT2017-83631-C3-R, and in part by the Nanotechnology in Translational Hyperthermia (HIPERNANO) under Grant RED2018–102626–T. The work of Elizabeth M. Jefremovas was supported by the Beca Concepción Arenal through the Gobierno de Cantabria–Universidad de Cantabria under Grant BDNS: 406333. The work of Irati Rodrigo was supported by the Programa de Perfeccionamiento de Personal Investigador Doctor (Gobierno Vasco) under Grant POS–2020–1–0028 and Grant IT–1005–16. The work of Lourdes Marcano was supported by the Postdoctoral Fellowship from the Basque Government under Grant POS–2019–2–0017.

ABSTRACT Magnetic Fluid Hyperthermia mediated by iron oxide nanoparticles is one of the most promising therapies for cancer treatment. Among the different candidates, magnetite and maghemite nanoparticles have revealed to be some of the most promising candidates due to both their performance and their biocompatibility. Nonetheless, up to date, the literature comparing the heating efficiency of magnetite and maghemite nanoparticles of similar size is scarce. To fill this gap, here we provide a comparison between commercial Synomag Nanoflowers (pure maghemite) and bacterial magnetosomes (pure magnetite) synthesized by the magnetotactic bacterium *Magnetospirillum gryphiswaldense* of $\langle D \rangle \approx 40$–45 nm. Both types of nanoparticles exhibit a high degree of crystallinity and an excellent degree of chemical purity and stability. The structural and magnetic properties in both nanoparticle ensembles have been studied by means of X–Ray Diffraction, Transmission Electron Microscopy, X–Ray Absorption Spectroscopy, and SQUID magnetometry. The heating efficiency has been analyzed in both systems using AC magnetometry at several field amplitudes (0–88 mT) and frequencies (130, 300, and 530 kHz).

INDEX TERMS Hyperthermia, nanoparticles, X–ray diffraction, magnetic properties.

I. INTRODUCTION

In recent years, there has been an increasing number of works on iron oxide based magnetic nanoparticles for different kinds of biomedical applications, such as Drug Delivery, Magnetic Resonance Imaging (MRI), Magnetic Particle Imaging (MPI), and Magnetic Hyperthermia [1]–[6]. Among these, Magnetic Hyperthermia, which is mediated by magnetic nanoparticles (MNPs), constitutes a promising approach for cancer treatment. The basic idea behind this treatment consists on delivering the MNPs to the tumor area so that, under the application of an external AC magnetic field with a frequency f ranging between 100 kHz and 1 MHz, the MNPs release heat in a localized way, thereby deactivating the cancer cells without affecting the healthy ones [7], [8]. Phase I clinical trials on magnetic hyperthermia were performed in

The associate editor coordinating the review of this manuscript and approving it for publication was Montserrat Rivas.

the early 2000s in Germany (MagForce Nanotechnologies, see [9]), and recently new trials have been approved for treatment of specific type of cancers (e.g. glioblastoma and prostate) in several countries around the world, including Japan, Germany, USA, and China [10]–[14].

Although different materials have been investigated as magnetic hyperthermia agents, iron oxide based MNPs have received most of the attention due to their chemical stability, high magnetization, relatively well–known metabolism, high biocompatibility, etc. [7], [15]. On top of that, some of the best heating results in magnetic hyperthermia have been reported for iron oxide based MNPs, with heating efficiency values (quantified by the Specific Absorption Rate, *SAR*) up to $SAR/f = 8$ W/gkHz in exchange coupled ferrites [16]–[18]. Nevertheless, the term ''iron oxide'' is generic and can encompass a wide range of different oxide phases, such as γ-Fe_2O_3 (maghemite), Fe_3O_4 (magnetite), α-Fe_2O_3 (hematite), FeO (wüstite), etc. [19]. Each one of these iron oxide phases presents different kinds of magnetic behavior, and therefore, a very different heating efficiency. As has been previously described [20], the heating efficiency of the MNPs is directly related to the ''hysteresis losses'' of the MNPs under an external AC field. These losses are proportional to the hysteresis loop area, and therefore, are directly related to the magnetic behavior of the MNPs. Although there have been a few reports on the heating efficiency of MNPs made of iron oxide phases such as FeO [21], ϵ–Fe_2O_3 [22] or α–Fe_2O_3 [23], most of the current articles are based on MNPs composed of magnetite and/or maghemite, since these compounds are the only ones approved by the United States Food and Drug Administration (FDA) and the European Medicines Agency (EMA) for clinical use.

Magnetite and maghemite are ferrimagnetic iron oxides with a similar cubic structure [24]. Magnetite presents a face–centered cubic spinel crystal structure with tetrahedral sites occupied by Fe^{3+} ions while octahedral sites are evenly filled by Fe^{2+} and Fe^{3+} ions. In stoichiometric magnetite, the ratio of Fe^{2+} and Fe^{3+} is 1:2. Magnetite phase tends to oxidize into maghemite upon exposure to oxygen, resulting in the conversion of all Fe^{2+} ions into Fe^{3+}. For the case of this stoichiometric magnetite, the ferrimagnetic moment arises from unpaired Fe^{2+} spins in octahedral sites, while in the case of maghemite, unpaired octahedral Fe^{3+} spins are the ones responsible for the magnetism [19], [25].

Since maghemite is a more stable iron oxide phase than magnetite, many of the MNPs developed for magnetic hyperthermia, especially commercial ones, are made either of maghemite, or a magnetite core and an oxidized maghemite shell [26]–[30]. For example, in a recent work, Bender *et al.* [31] showed that commercial maghemite Nanoflowers ($\langle D \rangle \sim 40$ nm), composed of several crystallites/cores, presented very high heating efficiency, SAR ($\mu_0 H = 8.8$ mT, $f = 939$ kHz) $= 322$ W/g, in comparison to other similar iron oxide based nanoparticles. On the other hand, pure magnetite nanoparticles are also very promising but generally they need to be coated with some kind of capping agent in order to prevent oxidation. Several works have studied their use for magnetic hyperthermia [17], [18], [32]. An interesting case is that of magnetosomes, pure magnetite MNPs synthesized by magnetotactic bacteria and intrinsically coated with a lipid bilayer. To this respect, recent works have reported very high heating efficiency values in these cube–octahedral magnetosomes of $\langle D \rangle \approx 45$ nm (SAR/f up to 5 W/gkHz) [33]–[37]. In both cases (NFs and BMs), several works ([38] or [39], respectively) have evidenced their high biocompatibility, as they can be almost completely assimilated by human cells once their therapeutic function is completed, being degraded afterwards. In addition, we must stress that although sometimes in the literature magnetite and maghemite are presented as ''interchangeable'' materials when referring to MNPs, due to their similar saturation magnetization ($M_{\text{sat Fe3O4}} \sim 92$ Am^2/kg and $M_{\text{sat } \gamma\text{–Fe2O3}} \sim 76$ Am^2/kg [25]), this is not entirely correct, given that these iron oxide phases do actually present several differences in their magnetic response (e.g. magnetic anisotropy, Verwey transition…), and this can affect their performance in different biomedical applications, including magnetic hyperthermia [40]. Therefore, a good characterization of the magnetic properties of magnetite/maghemite MNPs becomes mandatory [17], [41], [42].

Considering all this, in this work we have compared two of the most promising MNPs for magnetic hyperthermia: commercial maghemite Nanoflowers (NFs) and magnetite bacterial magnetosomes from *Magnetospirillum gryphiswaldense* (BMs). Both samples present similar size ($\langle D \rangle \sim 40$–$45$ nm), high crystallinity, and well defined morphology (multicore for the NFs and cube–octahedral for the BMs). We have analyzed their microstructure using X–Ray Diffraction (XRD) and Transmission Electron Microscopy (TEM), checked their composition by using X–ray Absorption Near Edge Spectroscopy (XANES) to ensure the chemical purity of each ensemble, studied their magnetic response with DC magnetometry, and finally compared their heating efficiency using AC magnetometry. To this respect, we have employed a novel home–made setup for AC magnetometry measurements, which has allowed us to measure the *SAR* of these MNPs at 3 different frequencies, applying AC fields up to 88 mT. This has allowed us to clearly depict the different heating ranges of these magnetite/maghemite MNPs, and also to obtain a landscape of the fields and frequencies that maximize their heating efficiency under certain safety limits.

II. MATERIALS AND METHODS

Commercial Synomag Nanoflowers were supplied by Micromod Partikeltechnologie GmbH (Germany). Each flower consists on Dextran–coated (~ 12 nm thickness) maghemite γ-Fe_2O_3 multicores (~ 10 cores/each). The multicore maghemite structure is of ~ 45 nm. These MNPs were synthesized following a polyol method [43], [44].

The magnetosomes employed in this study are magnetite Fe_3O_4 nanoparticles synthesized by magnetotactic bacteria

from the *Magnetospirillum gryphiswaldense* strain MSR-1 (DMSZ 6631). Bacteria were cultured microaerobically at 28°C for 48 hours in Flask Standard Medium, as described by Heyen and Schüler [45], supplemented with 100 μM iron (III)–citrate to support magnetosome formation. Briefly, culture was carried out in three 1 L-bottles at 28°C under microaerobic conditions (bottles loosely capped and without shaking). Cells were collected after 120 h when well–formed magnetosomes were present. BMs have been measured either in the whole cells (DC–magnetometry, XRD and XANES) or isolated from the bacteria (TEM, AC magnetometry). For the preparation of whole bacteria samples, the cells were harvested by centrifugation, fixed in 2% glutaraldehyde, and washed three times in mQ water. The fixed and washed cells were freeze-dryed, resulting in a powder sample. Complementary, magnetosomes were extracted following the protocol described by Grünberg *et al.* [46] with minor modifications. The cells were collected by centrifugation, suspended in 20 mM HEPES–4 mM EDTA (pH = 7.4), and disrupted using a French press at P = 1.4 kbar. The lysated cells were sonicated, promoting the separation of magnetosomes, and centrifuged at 600 g for 5 min, to remove cell debris. Then, magnetosomes were collected from the supernatant by magnetic separation and rinsed 10 times with 10 mM HEPES-200 mM NaCl (pH = 7.4). Finally, the isolated magnetosomes were re–dispersed in deionized water (pH 7.4), sterilized in autoclave (115°C, 15 min), and stored at 4°C. The stability of the magnetite magnetosomes against oxidation is secured during several weeks.

XRD measurements were performed at room temperature on Synomag NFs and freeze-dried bacteria using a Bruker D8 Advance diffractometer equipped with a high count rate Lynxeye detector. This detector reduces the total counting time, which constitutes a great advantage to minimize the possible deterioration of the samples. The diffractometer was used working on Bragg-Bentano geometry and Cu-Kα ($\lambda = 1.5418$ Å) radiation. Patterns were collected within the range $20° \leq 2\theta \leq 110°$ with a 0.02° increment.

TEM was performed on both Synomag NFs and BMs (extracted from the bacteria) adsorbed onto 300 mesh carbon-coated copper grids. TEM images were obtained with a JEOL JEM–14000Plus electron microscope at an accelerating voltage of 120 kV. The particle size distribution was analyzed using a standard software for digital electron microscope image processing, ImageJ [47].

XANES measurements were performed on Synomag NFs and on BMs located within the bacteria (whole cells). The main aim of these measurements was to access information concerning medium–range order, which allow us to clearly differentiate the oxidation state (phase identification) in both MNP ensembles, as XRD provides long–range order information [48]. Fe K–edge XAS measurements of the NFs were carried out at the BL22 CLAESS beamline of the ALBA synchrotron ($T = 77$ K) and at the XAFS beamline of the Elettra synchrotron (Trieste, Italy) (Room Temperature, RT). On the other hand, the BMs were measured at the XAFS beamline of the Elettra synchrotron at RT. In all cases, measurements were performed in transmission mode using a double Si crystal monochromator oriented in the (111) direction. A reference Fe–sample was measured for determining the position of the bacteria Fe–K edge ($E = 7112$ eV).

DC magnetization (M) measurements were performed on bacteria (obtained as described before), encapsulated in gelatin capsules. Data were collected using a Quantum Design QD-MPMS (SQUID) magnetometer in the temperature range of T = 5–300 K applying magnetic fields $\mu_0 H$ between 0.5 mT and 2.05 T. M *vs.* T curves were measured from 10 to 300 K, following the Zero Field-Cooling/Field-Cooling protocol (ZFC–FC): The samples were cooled in the absence of any external field from 300 K to 5 K. At 5 K a fixed magnetic field of 5 mT was applied and the magnetization was measured upon warming to 300 K (ZFC). With the field still on, the sample was cooled to 5 K and the magnetization was measured upon warming to 300 K (FC). M *vs.* $\mu_0 H$ loops were measured at 300 K applying fields up to 5 T. The high-sensitivity of the SQUID ($\sim 10^{-7}$ emu) allowed us to use small amounts of the MNPs (m = 12.3 mg in the case of the NFs and m = 0.9 mg of freeze-dried bacteria). Here again, we decided to keep the BMs intracellular to avoid oxidation process and magnetic interactions among the magnetosomes.

AC magnetometry characterization was performed on NFs and BMs extracted from the bacteria (i.e., isolated magnetosomes) using a versatile home–made magnetometer that generates high magnetic fields able to saturate the samples. This device is capable of working at a wide frequency range (100 kHz–1 MHz) with large field intensity: 90 mT at low frequency side and 35 mT at high frequency side. Further details on the set up can be found in [49].

III. RESULTS AND DISCUSSION

A. STRUCTURAL CHARACTERIZATION

Figure 1 shows the X–Ray Diffraction (XRD) patterns together with the Rietveld refinements (**a** and **b**) and two representative Transmission Electron Microscopy (TEM) images, with the size distribution on the right (**c** and **d**) corresponding to the γ–Fe_2O_3 NFs and the Fe_3O_4 BMs (freeze–dried bacteria for XRD and isolated magnetosomes for TEM).

The Rietveld refinements performed on the NFs (see Figure 1 **a**) are consistent with a single phase of cubic Fd–3m space group, with a lattice parameter a = 8.3451(3) Å, and a mean nanoparticle size of $\langle D_{\gamma-Fe2O3} \rangle = 50.0(4)$ nm for the whole MNP core. The calculations also provide information on the microstrain, where a minimal $\eta = 0.93(1)\%$ has been obtained, which is indicative of their good crystallinity. The achieved low Bragg factor $R_B = 3.6\%$ guarantees the reliability of the fitting. Given that all the XRD peaks are indexed with those corresponding solely to the γ–Fe_2O_3 phase [50], the XRD characterization indicates that NFs are mainly composed of maghemite. The TEM images of these NFs (Fig. 1 **c**) verify the multicore structure (flower–shape)

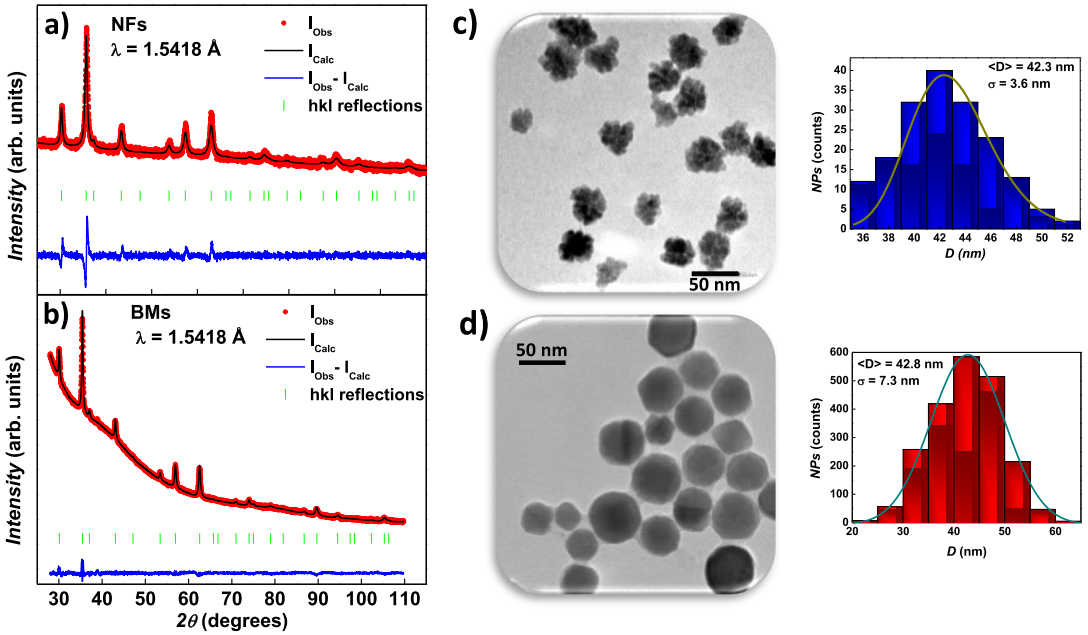

FIGURE 1. a) and b) include the XRD patterns together with the Rietveld refinements corresponding to the NFs and the BMs, respectively. The XRD patterns for the NFs are consistent with single phase of maghemite, whereas the positions for the Bragg peaks of the bacteria are consistent with a single phase of magnetite. In c) and d), two representative TEM images and size distribution are shown for NFs and BMs, respectively.

of each flower, where ~ 10 grains/core form the maghemite–core. A LogNormal size distribution with an average diameter $\langle D_{MNP} \rangle = 42.3$ nm and variance $\sigma = 3.6$ nm has been obtained from the analysis of the TEM images. This size is slightly smaller with respect to the one obtained by means of XRD, as expected [51].

On the other hand, the XRD pattern and Rietveld refinements ($R_B = 4.5\%$) performed on freeze–dried bacteria are shown in Fig. 1 **b**. The results are consistent with a single phase of cubic Fd–3m structure, with a = 8.3985(2) Å, which corresponds to magnetite [52]. No extra peaks apart from those corresponding to magnetite show up, which showcases the good crystallinity and the high chemical purity of the magnetosomes. The cell gives a contribution to the scattering intensity in the form of a background rise for $2\theta < 50°$. The Rietveld refinements point to a mean nano-crystallite size for magnetite $\langle D_{Fe3O4} \rangle = 45.1(3)$ nm. Here, an even lower microstrain $\eta = 0.384(2)\%$ is found, which ensures a minimal unit cell distortion, revealing the high crystallinity of the BMs. Fig. 1 **d** shows a TEM image corresponding to magnetosomes extracted from the bacteria. The analysis of the TEM images indicate a Gaussian size distribution centered in $\langle D_{MNP} \rangle = 42.8$ nm with $\sigma = 7.3$ nm, which is again slightly smaller with respect to the XRD one.

Although XRD can give us crystallographic information about the different iron oxide phases present in our samples, additional structural information can be obtained by XANES. XANES is a powerful technique that provides accurate data concerning the local environment and the oxidation state of the absorbing atoms, in our case, Fe [53]. Figure 2 shows the Fe K–edge ($E_0 = 7112$ eV) XANES spectra corresponding to **a)** the NFs and **b)** BMs within the bacteria, together with reference patterns of γ–Fe_2O_3 [54] and Fe_3O_4, and Linear Combination Fits (LCFs). These LCFs allow us to quantify the content of each Fe–phase in the samples, as it has been shown in previous studies (e.g., [55]).

According to the XANES spectrum plotted in Figure 2 **a)**, the edge position for the NFs, defined as the energy value at which the normalized absorption μ (E) reaches 0.5, is located at $E_0 \approx 7124$ eV, which is the typical value of maghemite, γ–Fe_2O_3 [54], [56]. LCFs indicate a perfect match between the reference γ–Fe_2O_3 pattern and the experimental XAS data corresponding to the NFs. This allow us to verify the chemical purity of the NFs that was pointed by XRD characterization. On the other hand, the XANES spectrum corresponding to the BMs (Fig.2 **b)**) is left-shifted in energy with respect to the NFs (edge position $E_0 \approx 7122$ eV, i.e., $\Delta E_0 \approx 2$ eV). This indicates a lower Fe–oxidation state, which is expected, as magnetite combines both Fe^{2+} and Fe^{3+}, whereas for maghemite, only Fe^{3+} is present [53], [57]. Here, the LCFs confirm the 100% magnetite–composition of the BMs. Therefore, we can unequivocally conclude that the NFs are fully composed of maghemite, whereas the BMs are fully composed of magnetite.

B. MAGNETIC CHARACTERIZATION

Figure 3 shows the magnetic characterization ($M(T, \mu_0 H)$) of both MNP ensembles. In Fig. 3 **a)**, the ZFC-FC curves measured at $\mu_0 H = 5$ mT can be inspected. First, concerning the NFs (blue squares), the ZFC and FC branches are separated in the whole temperature range, showcasing the high magnetic irreversibility of these Superparamagnetic (SPM)

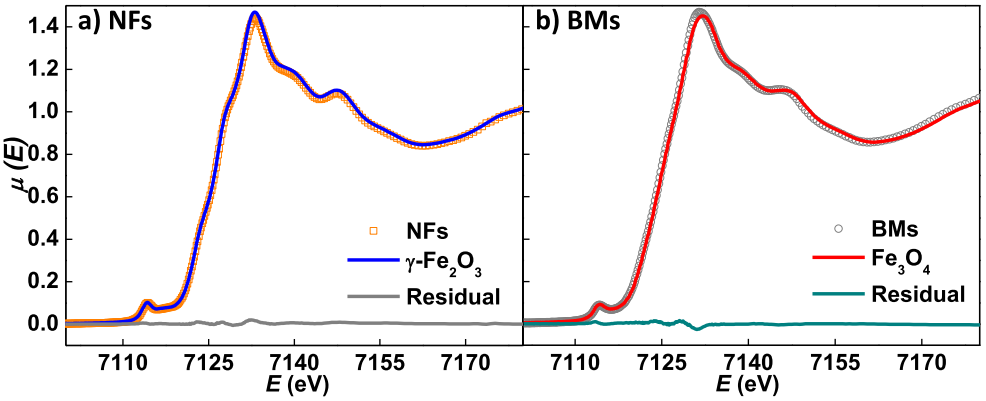

FIGURE 2. Normalized absorption μ (E) Fe K–edge XANES spectra corresponding to a) maghemite NFs and b) magnetite BMs. LCFs performed with reference XAS spectra corresponding to pure $\gamma-Fe_2O_3$ (blue) and Fe_3O_4 (red). The reliability of these LCFs can be checked by the residual lines (bottom), which are close to zero.

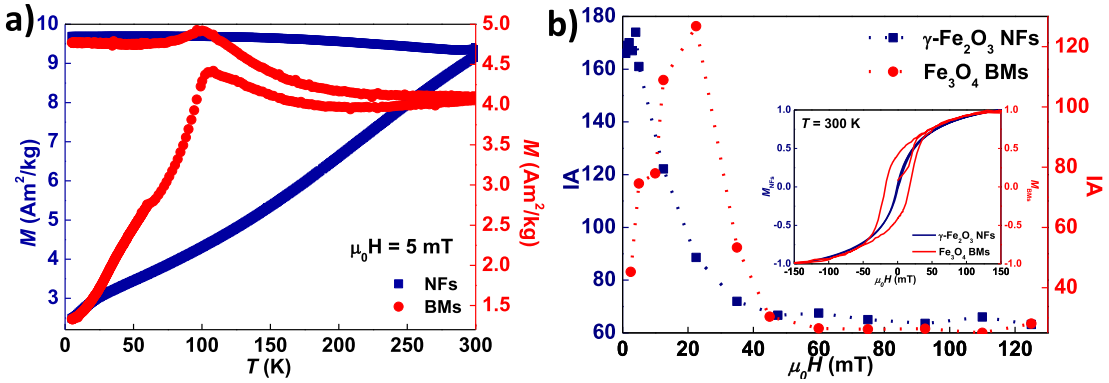

FIGURE 3. a) Zero Field Cooling-Field Cooling (ZFC-FC) $M(T)$ curves for $\gamma-Fe_2O_3$ NFs (blue circles) and Fe_3O_4 BMs (red squares) measured at $\mu_0 H = 5$ mT. In b), the evolution of the *IA* parameter *vs* the magnetic applied field $\mu_0 H$ is shown. It can be seen how the BMs achieve their maximum value at higher $\mu_0 H$ than the NFs. The inset shows the normalized hysteresis loops M/M_{sat} measured at $T = 300$ K.

MNPs [31]. On the other hand, the BMs (within the bacteria) (red circles), which are magnetically blocked at $T = 300$ K, evidence the expected Verwey transition, around $T_V \approx 106$ K, characteristic of Fe_3O_4. This transition is marked by a sudden drop of the magnetization with decreasing T. The T_V value agrees well with those previously reported for magnetosomes [57], [58] and it is found to be below the $T_V \sim 120$ K corresponding to bulk magnetite [59]. Needless to say, this Verwey transition is not present in the NFs, as expected for a pure maghemite system [31], [48]. Interestingly, the value of the magnetization measured at $T = 300$ K in the BMs ($M \approx 4.2$ Am^2/kg) is almost half the value corresponding to the NFs ($M \approx 9.8$ Am^2/kg). This would suggest a higher anisotropy barrier ($E_{\text{barrier}} \propto K \cdot V$) for the former. As both IONP ensembles are very close in size (i.e., very similar V), the BMs are revealing as an ensemble with higher anisotropy (K) with respect to the NFs. As has been reported in the literature, the effective anisotropy (K_{eff}) is a key parameter to optimize the heating efficiency of MNPs in magnetic hyperthermia ([25], [60]). Given that the interactions among the magnetic moments do affect this K_{eff}, we have analyzed the dependence of the Irreversibility Area parameter (*IA*, defined in [61]), with respect to the external applied field $\mu_0 H$ in the static regime. As described in [61], this parameter provides information on the *robustness* of the magnetic interactions among the magnetic moments, as the greater the interactions, the larger magnetic fields are needed to overcome the energy barriers between two spin states. The results, represented in Fig. 3 **b**, show that the BMs attain their maximum $IA = 174$ at $\mu_0 H = 12.5$ mT, whereas for the NFs, their maximum $IA = 127$ is achieved at $\mu_0 H = 4$ mT, i.e. a field three times larger is required to overcome the energy barrier in the case of the BMs. This result confirms the higher effective anisotropy of the BMs in comparison to NFs. The enhanced K_{eff} in the BMs can also be traced in the form of coercitivity ($\mu_0 H_C$) in the normalized hysteresis loops measured at $T = 300$ K (see inset in Fig. 3 **b**)). There, while the NFs exhibit a negligible value of $\mu_0 H_C$, the BMs show a value of $\mu_0 H_C \approx 20$ mT. On the other hand, another important parameter that determines the heating efficiency of the MNPs is the saturation magnetization M_{sat}. In our case, M_{sat} values obtained for NFs and BMs are ~ 63 and 92 Am^2/kg. A higher

M_{sat} value for BMs would in principle be an advantage for their use as magnetic hyperthermia agents, since it will give rise to higher hysteresis losses [62].

C. MAGNETIC FLUID HYPERTHERMIA

In order to study the heating efficiency of the NFs and the BMs (extracted from the bacteria), we have employed AC magnetometry measurements. AC magnetometry allows us to directly measure the AC hysteresis loops described by the magnetic moments of the nanoparticles in order to calculate their heating efficiency or *SAR* from the hysteresis losses associated. Previous works have demonstrated the heating efficiency of these MNP ensembles by measuring the Temperature vs time curves [62], [63] . The AC hysteresis loops measured for both NFs and BMs dispersed in water (concentration $\sim$ 3.1 mg/ml and $\sim$ 1.5 mg/ml respectively) are presented in Figure 4. These AC loops were measured at three different frequencies, f = 130, 300, and 530 kHz, with AC field amplitudes up to $\mu_0 H_{AC}$ = 88, 62, and 50 mT, respectively.

As depicted, the shape of the AC loops changes when increasing both the $\mu_0 H_{AC}$ and the f. Both samples exhibit narrow and elongated AC loops at low field amplitudes, i. e., the typical lancet shape [64]. This gives rise to low hysteresis losses and low heating efficiencies. Nonetheless, as the field amplitude increases, the AC loops become bigger and more squared until they reach a certain saturation at high enough fields, where the differences between the saturated loops are small. In addition, we can observe that the AC loops tend to become slightly wider and more squared at high enough field amplitudes.

If we compare both samples, quantitative differences are already seen, especially at high field amplitudes: the coercive field value, $\mu_0 H_{C-AC}$, is up to $\sim$ 85% higher for BMs than for NFs, and the $M_{\text{sat-AC}}$ is up to $\sim$ 26% higher. This suggests that the heating efficiency of BMs is going to be higher than NFs, especially in the high field region. In order to check this, *SAR* values have been calculated for both MNPs. These *SAR* values, in W/g, were directly obtained from the area, A, of the AC hysteresis loops according to the following equation:

$$SAR = \frac{f}{c} \cdot A = \frac{f}{c} \cdot \oint \mu_0 M_t dH_t \tag{1}$$

where M_t is the instantaneous magnetization at time t, H_t the sinusoidal magnetic field of frequency f at time t, and c is the magnetic material weight concentration in the dispersing medium.

SAR vs. $\mu_0 H_{AC}$ curves are shown in Figure 5. For both the NFs and the BMs, at field amplitudes below 5 mT, *SAR* values are nearly negligible. If we increase the field amplitude, the *SAR* starts increasing rapidly until a saturation is reached above a certain field, $\mu_0 H_{\text{sat}}$. As inserted in Table 1, the maximum *SAR* values obtained with BMs are appreciably higher ($>$ 100%) than those obtained for NFs, independently of the frequency. These differences can be essentially related to two parameters: the magnetic moment and the effective anisotropy of the MNPs.

TABLE 1. Values corresponding to the different parameters obtained from Figures 4 and 5 for the NFs and BMs measured at f = 130, 300 and 530 kHz. Errors for the values are below 5%.

	NFs			BMs		
f (kHz)	**130**	**300**	**530**	**130**	**300**	**530**
$SAR_{\max}$ (W/g)	370	930	1820	880	2120	4120
K_{eff} (kJ/m^3)	4.0	4.6	5.1	9.8	11.0	12.1
SAR_{limit} (W/g)	335	455	350	805	1125	570

Concerning the remanence and the coercive field, the BMs display greater values than the NFs. This can be related to differences in the effective anisotropy, K_{eff}, of both MNPs, as was already inferred from DC magnetic measurements. In order to get an estimation of K_{eff}, we can use the approach described by Mehdaoui *et al.* [64]. According to their model, an estimation of K_{eff} from the coercive field values, H_C, of the AC hysteresis loops, can be obtained using the following equation:

$$\mu_0 H_C = 0.96 \cdot \mu_0 H_\kappa (1 - \kappa^{0.8}) \tag{2}$$

where $H_\kappa = 2K_{\text{eff}}/\mu_0 M_{sat}$ is the anisotropy field, being κ a parameter given by:

$$\kappa = \frac{k_B T}{K_{eff} V} ln\left(\frac{k_B T}{4\mu_0 H_{max} M_{sat} V f \tau_0}\right) \tag{3}$$

where $\tau_0 = 10^{-10}$ s, $\mu_0 H_{\max}$ is the maximum applied field, and V is the MNP volume.

Using this expression, the magnetic anisotropy, K_{eff}, can be estimated for our BMs and NFs, as indicated in Table 1. The K_{eff} values obtained for these magnetosomes lie within the range of values typically reported for other highly crystalline magnetite nanoparticles of similar size [18], [34]. As observed, the higher effective anisotropy of BMs gives rise to wider AC loops, and thereby to higher hysteresis losses. This is valid, as has been explained before [65], [66], if the applied fields are strong enough: $\mu_0 H_{AC} \gg \mu_0 H_{\text{c-hyp}}$, being $\mu_0 H_{\text{c-hyp}}$ the field amplitude reached at the inflection point of the SAR vs field curve [65], [66].

Therefore, these two factors, higher magnetic moment and higher effective anisotropy, give an advantage to BMs, compared to NFs, in terms of heating efficiency.

Finally, for clinical applications it is important to consider certain safety limits in the value of the field amplitude and frequency in order to avoid producing non-specific heating in the body that can harm the patient. In the literature, different safety limits have been proposed. According to the so called Atkinson-Brezovich criterion, $H \cdot f$ should be lower than $4.85{\cdot}10^8$ A m^{-1}s^{-1} [67], [68], while following the Hergt criterion, which has become a more accepted estimation, this limit is ten times higher, $\sim 5 \cdot 10^9$ A m^{-1}s^{-1} [69]. At this point, it is worth mentioning that the Hergt criterion does not take into account the exposed volume to the magnetic field. Thus, in order to avoid the possible inductance of damaging

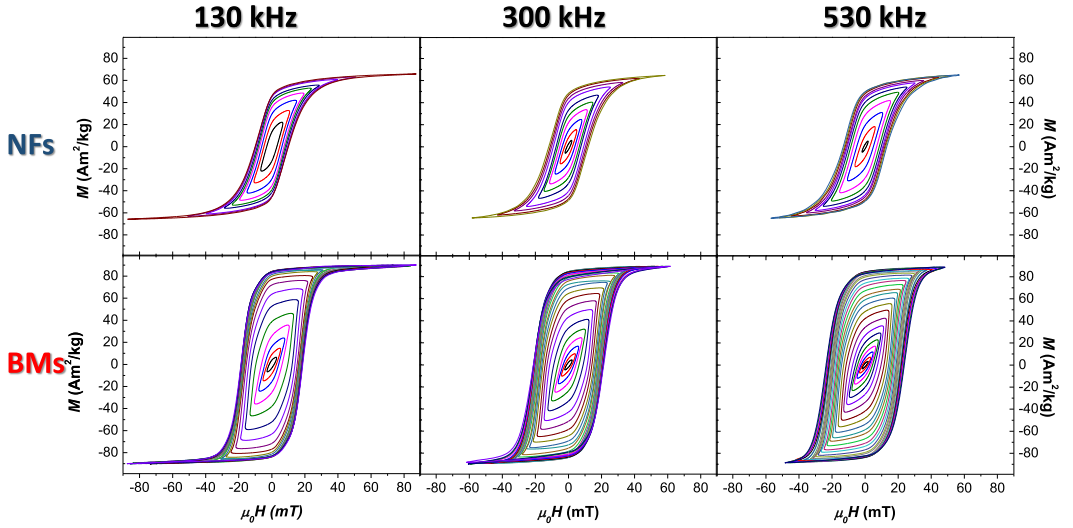

FIGURE 4. AC hysteresis loops measured for the NFs and the BMs (extracted from the bacteria) at three different frequencies, $f = 130$, 300 and 530 kHz, with AC field amplitudes up to $\mu_0 H_{AC} = 88$, 62, and 50 mT, respectively.

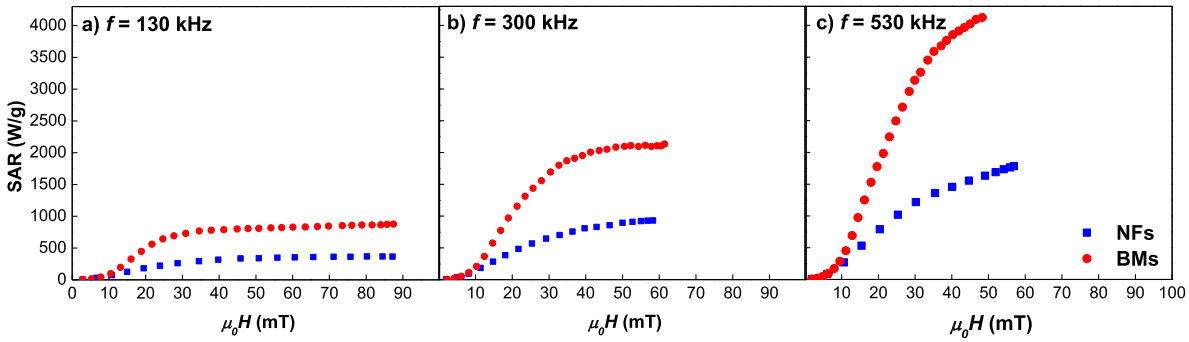

FIGURE 5. *SAR vs.* $\mu_0 H_{AC}$ curves for the NFs (blue squares) and the BMs (red circles) measured at a) $f = 130$, b) $f = 300$, and c) $f = 530$ kHz, with AC field amplitudes up to $\mu_0 H_{AC} = 88$, 61.5, and 50 mT, respectively. In all of the cases, the *SAR* corresponding to the BMs is more than twice the one of the NFs at high fields.

eddy currents connected to the use of high field amplitudes and/or frequencies, either the volume of exposed tissue or the heating time should be reduced. Following this Hergt criterion, the maximum achievable *SAR* of our samples can be calculated. As indicated in Table 1, both samples achieve their maximum SAR_{limit} at $f = 300$ kHz ($\mu_0 H_{\text{limit}} = 20.7$ mT), reaching a value of 455 W/g and 1125 W/g for NFs and BMs, respectively. The latter SAR_{limit} for BMs compares well with the reported ones found in the literature (e.g. [34]). A larger SAR_{limit} for BMs again supports the use of magnetite based NPs for maximizing the heating efficiency in magnetic hyperthermia under clinical conditions. Nevertheless, at this stage, it should be reminded that Synomag NFs have been blatantly presenting a high performance compared to other more conventional iron oxide nanoparticles synthesized by artificial routes. Such output is surely connected to the fact that there is some degree of spin disorder and exchange coupling in their nanometric scale, which altogether promote a large figure of merit for biomedical purposes [31]. The fact that they are commercially available demonstrates its technological interest, reasonable yield in large–scale production processes and high reproducibility. In addition, those Synomag NFs may also be relevant for customized surface modifications. All in all, it holds true that the magnetite BMs present a higher hyperthermia performance compared to maghemite NFs. Nevertheless, the conditions of reproducibility and large–scale production of such biological MNPs are to be better defined, whereas Synomag NFs constitute already a high–available technological advanced product.

IV. CONCLUSION

Magnetosomes synthesized by the magnetotactic bacterium *M. gryphiswaldense* have revealed better performance for Magnetic Fluid Hyperthermia purposes with respect to commercial Synomag Nanoflowers. The higher effective anisotropy and saturation magnetization of BMs give rise to higher heating efficiency in comparison to NFs in all the range of field amplitudes and frequencies analyzed. In this way, it has been shown that the maximum *SAR* attainable under clinical conditions, SAR_{limit}, is nearly 2.5 higher in

BMs with respect to Synomag NFs, which are already considered an outstanding candidate for Magnetic Hyperthermia Therapy. In the case of BMs, the process of getting commercial amounts is the next challenge to be faced, as they are still far from the production of these Synomag NFs, whose fabrication process is well–standardized. The work presented here is also opening a research line aiming to compare Magnetic Hyperthermia Therapy performance in promising candidates by both AC magnetometry and calorimetric methods. Finally, the fact that both NFs and BMs can be almost totally assimilated and degraded by human cells is, indeed, a strong point for their clinical use and a key factor to their long–term biocompatibility.

ACKNOWLEDGMENT

The authors would like to thank the ALBA and Elettra synchrotron radiation facilities and staff for the allocation of beamtime and assistance during the experiments.

REFERENCES

[1] W. Wu, Z. Wu, T. Yu, C. Jiang, and W.-S. Kim, "Recent progress on magnetic iron oxide nanoparticles: Synthesis, surface functional strategies and biomedical applications," *Sci. Technol. Adv. Mater.*, vol. 16, no. 2, Apr. 2015, Art. no. 023501.

[2] A. Figuerola, R. Di Corato, L. Manna, and T. Pellegrino, "From iron oxide nanoparticles towards advanced iron-based inorganic materials designed for biomedical applications," *Pharmacol. Res.*, vol. 62, no. 2, pp. 126–143, Aug. 2010.

[3] S. Laurent, S. Dutz, U. O. Häfeli, and M. Mahmoudi, "Magnetic fluid hyperthermia: Focus on superparamagnetic iron oxide nanoparticles," *Adv. Colloid Interface Sci.*, vol. 166, nos. 1–2, pp. 8–23, Aug. 2011.

[4] Q. A. Pankhurst, N. T. K. Thanh, S. K. Jones, and J. Dobson, "Progress in applications of magnetic nanoparticles in biomedicine," *J. Phys. D, Appl. Phys.*, vol. 42, no. 22, Nov. 2009, Art. no. 224001.

[5] E. Alphandéry, "Natural metallic nanoparticles for application in nano-oncology," *Int. J. Mol. Sci.*, vol. 21, no. 12, p. 4412, Jun. 2020.

[6] E. Alphandéry, "Bio-synthesized iron oxide nanoparticles for cancer treatment," *Int. J. Pharmaceutics*, vol. 586, Aug. 2020, Art. no. 119472.

[7] D. Ortega and Q. A. Pankhurst, "Magnetic hyperthermia," *Nanoscience*, vol. 1, no. 60, p. e88, 2013.

[8] E. A. Périgo, G. Hemery, O. Sandre, D. Ortega, E. Garaio, F. Plazaola, and F. J. Teran, "Fundamentals and advances in magnetic hyperthermia," *Appl. Phys. Rev.*, vol. 2, no. 4, 2015, Art. no. 041302.

[9] *See*. Accessed: Apr. 2021. [Online]. Available: https://www.magforce.com/for additional information and [Online]. Available: https://www.magforce.com/home/

[10] S. Luo, L. Wang, W. Ding, H. Wang, J. Zhou, H. Jin, S. Su, and W. Ouyang, "Clinical trials of magnetic induction hyperthermia for treatment of tumours," *OA Cancer*, vol. 2, no. 2, pp. 1–6, 2014.

[11] E. Cazares-Cortes, S. Cabana, C. Boitard, E. Nehlig, N. Griffete, J. Fresnais, C. Wilhelm, A. Abou-Hassan, and C. Ménager, "Recent insights in magnetic hyperthermia: From the 'hot-spot' effect for local delivery to combined magneto-photo-thermia using magneto-plasmonic hybrids," *Adv. Drug Del. Rev.*, vol. 138, pp. 233–246, Jan. 2019.

[12] I. Rubia-Rodríguez, A. Santana-Otero, and S. Spassov, "Whither magnetic hyperthermia? A tentative roadmap," *Materials*, vol. 14, no. 4, p. 706, Feb. 2021.

[13] A. C. Anselmo and S. Mitragotri, "A review of clinical translation of inorganic nanoparticles," *AAPS J.*, vol. 17, no. 5, pp. 1041–1054, Sep. 2015.

[14] B. Thiesen and A. Jordan, "Clinical applications of magnetic nanoparticles for hyperthermia," *Int. J. Hyperthermia*, vol. 24, no. 6, pp. 467–474, 2008.

[15] S. Laurent, C. Burtea, C. Thirifays, U. O. Häfeli, and M. Mahmoudi, "Crucial ignored parameters on nanotoxicology: The importance of toxicity assay modifications and 'cell vision,'" *PLoS ONE*, vol. 7, no. 1, 2012, Art. no. e29997.

[16] J.-H. Lee, J.-T. Jang, J.-S. Choi, S. H. Moon, S.-H. Noh, J.-W. Kim, J.-G. Kim, I.-S. Kim, K. I. Park, and J. Cheon, "Exchange-coupled magnetic nanoparticles for efficient heat induction," *Nature Nanotechnol.*, vol. 6, no. 7, pp. 418–422, Jul. 2011.

[17] Z. Nemati, J. Alonso, I. Rodrigo, R. Das, E. Garaio, J. Á. García, I. Orue, M.-H. Phan, and H. Srikanth, "Improving the heating efficiency of iron oxide nanoparticles by tuning their shape and size," *J. Phys. Chem. C*, vol. 122, no. 4, pp. 2367–2381, Feb. 2018.

[18] I. Castellanos-Rubio, I. Rodrigo, R. Munshi, O. Arriortua, J. S. Garitaonandia, A. Martinez-Amesti, F. Plazaola, I. Orue, A. Pralle, and M. Insausti, "Outstanding heat loss via nano-octahedra above 20 nm in size: From wustite-rich nanoparticles to magnetite single-crystals," *Nanoscale*, vol. 11, no. 35, pp. 16635–16649, 2019.

[19] D. Faivre, *Iron Oxides: From Nature to Applications*. Hoboken, NJ, USA: Wiley, 2016.

[20] J. Carrey, B. Mehdaoui, and M. Respaud, "Simple models for dynamic hysteresis loop calculations of magnetic single-domain nanoparticles: Application to magnetic hyperthermia optimization," *J. Appl. Phys.*, vol. 109, no. 8, 2011, Art. no. 083921.

[21] H. Khurshid, J. Alonso, Z. Nemati, M. Phan, P. Mukherjee, M. Fdez-Gubieda, J. Barandiarán, and H. Srikanth, "Anisotropy effects in magnetic hyperthermia: A comparison between spherical and cubic exchange-coupled FeO/Fe_3O_4 nanoparticles," *J. Appl. Phys.*, vol. 117, no. 17, 2015, Art. no. 17A337.

[22] Y. Gu, M. Yoshikiyo, A. Namai, D. Bonvin, A. Martinez, R. Piñol, P. Téllez, and N. J. O. Silva, "Magnetic hyperthermia with ε-Fe_2O_3 nanoparticles," *Rsc Adv.*, vol. 10, no. 48, pp. 28786–28797, 2020.

[23] M. A. Zayed, M. A. Ahmed, N. G. Imam, and D. H. El Sherbiny, "Preparation and structure characterization of hematite/magnetite ferro-fluid nanocomposites for hyperthermia purposes," *J. Mol. Liquids*, vol. 222, pp. 895–905, Oct. 2016.

[24] R. M. Cornell and U. Schwertmann, *The Iron Oxides: Structure, Properties, Reactions, Occurrences and Uses*. Hoboken, NJ, USA: Wiley, 2003.

[25] B. D. Cullity and C. D. Graham, *Introduction to Magnetic Materials*. Hoboken, NJ, USA: Wiley, 2011.

[26] E. M. Múzquiz-Ramos, V. Guerrero-Chávez, B. I. Macías-Martínez, C. M. López-Badillo, and L. A. García-Cerda, "Synthesis and characterization of maghemite nanoparticles for hyperthermia applications," *Ceram. Int.*, vol. 41, no. 1, pp. 397–402, Jan. 2015.

[27] M. Lévy, C. Wilhelm, J.-M. Siaugue, O. Horner, J.-C. Bacri, and F. Gazeau, "Magnetically induced hyperthermia: Size-dependent heating power of γ-Fe_2O_3 nanoparticles," *J. Phys., Condens. Matter*, vol. 20, no. 20, 2008, Art. no. 204133.

[28] K. Simeonidis, C. Martinez-Boubeta, D. Serantes, S. Ruta, O. Chubykalo-Fesenko, R. Chantrell, J. Oró-Solé, L. Balcells, A. S. Kamzin, R. A. Nazipov, A. Makridis, and M. Angelakeris, "Controlling magnetization reversal and hyperthermia efficiency in core–shell iron–iron oxide magnetic nanoparticles by tuning the interphase coupling," *ACS Appl. Nano Mater.*, vol. 3, no. 5, pp. 4465–4476, 2020.

[29] R. Hergt, R. Hiergeist, I. Hilger, W. A. Kaiser, Y. Lapatnikov, S. Margel, and U. Richter, "Maghemite nanoparticles with very high AC-losses for application in RF-magnetic hyperthermia," *J. Magn. Magn. Mater.*, vol. 270, no. 3, pp. 345–357, Apr. 2004.

[30] A. Curcio, A. K. Silva, S. Cabana, A. Espinosa, B. Baptiste, N. Menguy, C. Wilhelm, and A. Abou-Hassan, "Iron oxide nanoflowers@ CuS hybrids for cancer tri-therapy: Interplay of photothermal therapy, magnetic hyperthermia and photodynamic therapy," *Theranostics*, vol. 9, no. 5, p. 1288, 2019.

[31] P. Bender, J. Fock, C. Frandsen, M. F. Hansen, C. Balceris, F. Ludwig, O. Posth, E. Wetterskog, L. K. Bogart, P. Southern, W. Szczerba, L. Zeng, K. Witte, C. Grüttner, F. Westphal, D. Honecker, D. González-Alonso, L. Fernández Barquín, and C. Johansson, "Relating magnetic properties and high hyperthermia performance of iron oxide nanoflowers," *J. Phys. Chem. C*, vol. 122, no. 5, pp. 3068–3077, Feb. 2018.

[32] R. Das, J. Alonso, Z. Nemati Porshokouh, V. Kalappattil, D. Torres, M.-H. Phan, E. Garaio, J. A. García, J. L. Sanchez Llamazares, and H. Srikanth, "Tunable high aspect ratio iron oxide nanorods for enhanced hyperthermia," *J. Phys. Chem. C*, vol. 120, no. 18, pp. 10086–10093, 2016.

[33] A. S. Mathuriya, "Magnetotactic bacteria for cancer therapy," *Biotechnol. Lett.*, vol. 37, no. 3, pp. 491–498, Mar. 2015.

[34] A. Muela, D. Muñoz, R. Martín-Rodríguez, I. Orue, E. Garaio, A. Abad Díaz de Cerio, J. Alonso, J. Á. García, and M. L. Fdez-Gubieda, "Optimal parameters for hyperthermia treatment using biomineralized magnetite nanoparticles: Theoretical and experimental approach," *J. Phys. Chem. C*, vol. 120, no. 42, pp. 24437–24448, Oct. 2016.

[35] M. L. Fdez-Gubieda, J. Alonso, A. García-Prieto, A. García-Arribas, L. Fernández Barquín, and A. Muela, "Magnetotactic bacteria for cancer therapy," *J. Appl. Phys.*, vol. 128, no. 7, Aug. 2020, Art. no. 070902.

[36] E. Alphandéry, "Applications of magnetosomes synthesized by magnetotactic bacteria in medicine," *Frontiers Bioengineering Biotechnol.*, vol. 2, p. 5, Mar. 2014.
[37] A. Edouard, "Applications of magnetotactic bacteria and the magnetosome for cancer treatment," in *Drug Discovery Today*. London, U.K.: Wiley, 2020, pp. S1359–S6446.
[38] F. Mazuel, A. Espinosa, G. Radtke, M. Bugnet, S. Neveu, Y. Lalatonne, G. A. Botton, A. Abou-Hassan, and C. Wilhelm, "Magneto-thermal metrics can mirror the long-term intracellular fate of magneto-plasmonic nanohybrids and reveal the remarkable shielding effect of gold," *Adv. Funct. Mater.*, vol. 27, no. 9, Mar. 2017, Art. no. 1605997.
[39] A. Curcio, A. Van de Walle, A. Serrano, S. Preveral, C. Péchoux, D. Pignol, N. Menguy, C. T. Lefevre, A. Espinosa, and C. Wilhelm, "Transformation cycle of magnetosomes in human stem cells: From degradation to biosynthesis of magnetic nanoparticles anew," *ACS Nano*, vol. 14, no. 2, pp. 1406–1417, Feb. 2020.
[40] S. Cabana, A. Curcio, A. Michel, C. Wilhelm, and A. Abou-Hassan, "Iron oxide mediated photothermal therapy in the second biological window: A comparative study between magnetite/maghemite nanospheres and nanoflowers," *Nanomaterials*, vol. 10, no. 8, p. 1548, Aug. 2020.
[41] G. F. Goya, E. Lima, Jr, A. D. Arelaro, T. Torres, H. R. Rechenberg, L. Rossi, C. Marquina, and M. R. Ibarra, "Magnetic hyperthermia with Fe_3O_4 nanoparticles: The influence of particle size on energy absorption," *IEEE Trans. Magn.*, vol. 44, no. 11, pp. 4444–4447, Nov. 2008.
[42] G. C. Lavorato, R. Das, Y. Xing, J. Robles, F. J. Litterst, E. Baggio-Saitovitch, M.-H. Phan, and H. Srikanth, "Origin and shell-driven optimization of the heating power in core/shell bimagnetic nanoparticles," *ACS Appl. Nano Mater.*, vol. 3, no. 2, pp. 1755–1765, Feb. 2020.
[43] H. Gavilán, A. Kowalski, and D. Heinke, "Colloidal flower-shaped iron oxide nanoparticles: Synthesis strategies and coatings," *Part. Part. Syst. Characterization*, vol. 34, no. 7, Jul. 2017, Art. no. 1700094.
[44] L. Lartigue, P. Hugounenq, D. Alloyeau, S. P. Clarke, M. Levy, J.-C. Bacri, R. Bazzi, D. F. Brougham, C. Wilhelm, and F. Gazeau, "Cooperative organization in iron oxide multi-core nanoparticles potentiates their efficiency as heating mediators and MRI contrast agents," *ACS Nano*, vol. 6, no. 12, pp. 10935–10949, Dec. 2012.
[45] U. Heyen and D. Schüler, "Growth and magnetosome formation by microaerophilic magnetospirillum strains in an oxygen-controlled fermentor," *Appl. Microbiol. Biotechnol.*, vol. 61, nos. 5–6, pp. 536–544, Jun. 2003.
[46] K. Grünberg, C. Wawer, B. M. Tebo, and D. Schüler, "A large gene cluster encoding several magnetosome proteins is conserved in different species of magnetotactic bacteria," *Appl. Environ. Microbiol.*, vol. 67, no. 10, pp. 4573–4582, Oct. 2001.
[47] C. A. Schneider, W. S. Rasband, and K. W. Eliceiri, "NIH image to imageJ: 25 years of image analysis," *Nature Methods*, vol. 9, no. 7, pp. 671–675, 2012.
[48] A. Espinosa, A. Serrano, A. Llavona, J. Jimenez de la Morena, M. Abuin, A. Figuerola, T. Pellegrino, J. F. Fernández, M. Garcia-Hernandez, G. R. Castro, and M. A. Garcia, "On the discrimination between magnetite and maghemite by XANES measurements in fluorescence mode," *Meas. Sci. Technol.*, vol. 23, no. 1, Jan. 2012, Art. no. 015602.
[49] I. Rodrigo, I. Castellanos-Rubio, E. Garaio, O. K. Arriortua, M. Insausti, I. Orue, J. Á. García, and F. Plazaola, "Exploring the potential of the dynamic hysteresis loops via high field, high frequency and temperature adjustable AC magnetometer for magnetic hyperthermia characterization," *Int. J. Hyperthermia*, vol. 37, no. 1, pp. 976–991, Jan. 2020.
[50] C. J. Serna, F. Bødker, S. Mørup, M. P. Morales, F. Sandiumenge, and S. Veintemillas-Verdaguer, "Spin frustration in maghemite nanoparticles," *Solid State Commun.*, vol. 118, no. 9, pp. 437–440, May 2001.
[51] H. Jensen, J. H. Pedersen, J. Jørgensen, J. S. Pedersen, K. D. Joensen, S. B. Iversen, and E. Søgaard, "Determination of size distributions in nanosized powders by TEM, XRD, and SAXS," *J. Exp. Nanosci.*, vol. 1, no. 3, pp. 355–373, 2006.
[52] J. Yoshida and S. Iida, "X-ray study of the phase transition in magnetite," *J. Phys. Soc. Jpn.*, vol. 47, no. 5, pp. 1627–1633, Nov. 1979.
[53] M. L. Fdez-Gubieda, A. García-Prieto, J. Alonso, and C. Meneghini, "X-ray absorption fine structure spectroscopy in fe oxides and oxyhydroxides," in *Iron Oxides*. Amsterdam, The Netherlands: Elsevier, 2016, pp. 397–422.
[54] A. Corrias, G. Ennas, G. Mountjoy, and G. Paschina, "An X-ray absorption spectroscopy study of the Fe K edge in nanosized maghemite and in Fe_2O_3–SiO_2 nanocomposites," *Phys. Chem. Chem. Phys.*, vol. 2, no. 5, pp. 1045–1050, 2000.
[55] D. Muñoz, L. Marcano, R. Martín-Rodríguez, L. Simonelli, A. Serrano, A. García-Prieto, M. L. Fdez-Gubieda, and A. Muela, "Magnetosomes could be protective shields against metal stress in magnetotactic bacteria," *Sci. Rep.*, vol. 10, no. 1, pp. 1–12, Dec. 2020.
[56] M. Wilke, F. Farges, P.-E. Petit, G. E. Brown, Jr, and F. Martin, "Oxidation state and coordination of Fe in minerals: An Fe *K-XANES* spectroscopic study," *Amer. Mineralogist*, vol. 86, nos. 5–6, pp. 714–730, 2001.
[57] M. L. Fdez-Gubieda, A. Muela, J. Alonso, A. García-Prieto, L. Olivi, R. Fernandez-Pacheco, and J. M. Barandiarán, "Magnetite biomineralization in *Magnetospirillum gryphiswaldense*: Time-resolved magnetic and structural studies," *ACS Nano*, vol. 7, no. 4, pp. 3297–3305, 2013.
[58] R. Prozorov, T. Prozorov, S. K. Mallapragada, B. Narasimhan, T. J. Williams, and D. A. Bazylinski, "Magnetic irreversibility and the verwey transition in nanocrystalline bacterial magnetite," *Phys. Rev. B, Condens. Matter*, vol. 76, no. 5, Aug. 2007, Art. no. 054406.
[59] F. Walz, "The Verwey transition-a topical review," *J. Phys., Condens. Matter*, vol. 14, no. 12, p. R285, 2002.
[60] D. Fiorani, A. M. Testa, F. Lucari, F. D'Orazio, and H. Romero, "Magnetic properties of maghemite nanoparticle systems: Surface anisotropy and interparticle interaction effects," *Phys. B, Condens. Matter*, vol. 320, nos. 1–4, pp. 122–126, Jul. 2002.
[61] E. M. Jefremovas, J. Alonso, M. de la Fuente Rodríguez, J. Rodríguez Fernández, J. I. Espeso, D. P. Rojas, A. García-Prieto, M. L. Fernández-Gubieda, and L. Fernández Barquín, "Investigating the size and microstrain influence in the magnetic order/disorder state of $GdCu_2$ nanoparticles," *Nanomaterials*, vol. 10, no. 6, p. 1117, Jun. 2020.
[62] D. Gandia, L. Gandarias, I. Rodrigo, J. Robles-García, R. Das, E. Garaio, J. Á. García, M. Phan, H. Srikanth, I. Orue, J. Alonso, A. Muela, and M. L. Fdez-Gubieda, "Unlocking the potential of magnetotactic bacteria as magnetic hyperthermia agents," *Small*, vol. 15, no. 41, Oct. 2019, Art. no. 1902626.
[63] S. Shaw, J. Kailashiya, A. Gangwar, S. Alla, S. K. Gupta, C. Prajapat, S. S. Meena, D. Dash, P. Maiti, and N. Prasad, "γ-Fe_2O_3 nanoflowers as efficient magnetic hyperthermia and photothermal agent," *Appl. Surf. Sci.*, vol. 560, Sep. 2021, Art. no. 150025.
[64] B. Mehdaoui, R. P. Tan, A. Meffre, J. Carrey, S. Lachaize, B. Chaudret, and M. Respaud, "Increase of magnetic hyperthermia efficiency due to dipolar interactions in low-anisotropy magnetic nanoparticles: Theoretical and experimental results," *Phys. Rev. B, Condens. Matter*, vol. 87, no. 17, May 2013, Art. no. 174419.
[65] N. A. Usov and B. Y. Liubimov, "Dynamics of magnetic nanoparticle in a viscous liquid: Application to magnetic nanoparticle hyperthermia," *J. Appl. Phys.*, vol. 112, no. 2, 2012, Art. no. 023901.
[66] I. Conde-Leboran, D. Baldomir, C. Martinez-Boubeta, O. Chubykalo-Fesenko, M. del Puerto Morales, G. Salas, D. Cabrera, J. Camarero, F. J. Teran, and D. Serantes, "A single picture explains diversity of hyperthermia response of magnetic nanoparticles," *J. Phys. Chem. C*, vol. 119, no. 27, pp. 15698–15706, Jul. 2015.
[67] W. J. Atkinson, I. A. Brezovich, and D. P. Chakraborty, "Usable frequencies in hyperthermia with thermal seeds," *IEEE Trans. Biomed. Eng.*, vol. BME-31, no. 1, pp. 70–75, Jan. 1984.
[68] I. A. Brezovich, "Low frequency hyperthermia: Capacitive and ferromagnetic thermoseed methods," *Med. Phys. Monogr*, vol. 16, pp. 82–111, Jan. 1988.
[69] R. Hergt, S. Dutz, and M. Zeisberger, "Validity limits of the Néel relaxation model of magnetic nanoparticles for hyperthermia," *Nanotechnology*, vol. 21, no. 1, 2009, Art. no. 015706.

ELIZABETH M. JEFREMOVAS was born in Santander, Spain, in 1994. She received the B.S. degree in physics from the Universidad de Cantabria, in 2017, and the M.Sc. degree in nanophysics and advanced materials from the Universidad Complutense de Madrid, in 2018. She is currently pursuing the Ph.D. degree in nanomagnetism under the supervision of Prof. Luis Fernández Barquín with the Universidad de Cantabria granted with a "Concepción Arenal" Fellowship (Universidad de Cantabria–Gobierno de Cantabria).

Her current research interests include study of 4f and biocompatible Fe–oxides magnetic nanoparticles for basic research and their potential applications.

LUCÍA GANDARIAS was born in Bilbao, Spain, in 1994. She received the B.S. degree in biotechnology from the Universidad del País Vasco (UPV–EHU), in 2016, and the M.Sc. degree in biomaterials and tissue engineering from the University College London, in 2017. She is currently pursuing the Ph.D. degree in bionanomagnetism under the supervision of Prof. Alicia Muela and Dr. Ana García–Prieto with the UPV–EHU granted with a Spanish Government Fellowship (FPI).

Her current research interests include magnetotactic bacteria and their use in biomedical applications, such as magnetic hyperthermia and drug delivery.

IRATI RODRIGO was born in Bilbao, Spain, in 1989. She received the B.S. degree in physics and the B.S. degree in electronic engineering, the M.Sc. degree in biomedical engineering, and the Ph.D. degree from the Universidad del País Vasco (UPV–EHU), in 2015, 2016, and 2021, respectively.

She has authored more than ten scientific articles, and developed a high field, high frequency, and temperature adjustable AC magnetometer for magnetic hyperthermia characterization.

LOURDES MARCANO was born in Bilbao, Spain, in 1991. She received the B.S. degree in physics from the Universidad de Oviedo, in 2013, and the M.Sc. degree in new materials and the Ph.D. degree from the Universidad del País Vasco (UPV–EHU), in 2014 and 2018, respectively.

She has authored over 15 scientific articles, the vast majority focused on the study of magnetotactic bacteria.

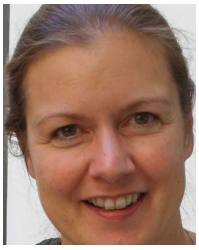

CORDULA GRÜTTNER developed a Postdoctoral Research with the Institute of Inorganic and Analytical Chemistry, Johannes Gutenberg–Universität Mainz, from 1993 to 1995. Since 1996, she has been a Principal Scientist with the Research and Development, Micromod Partikeltechnologie GmbH. She has authored more than 90 scientific articles and filed up to five patents related to the synthesis process of magnetic nanoparticles.

JOSÉ ÁNGEL GARCÍA is currently a Senior Professor with the Physics Department, Universidad del País Vasco (UPV–EHU). He has led more than 17 scientific projects in the last ten years. He has authored more than 100 publications in the last decade.

ENEKO GARAYO (Member, IEEE) is currently an Assistant Professor with the Department of Applied Physics, Universidad Pública de Navarra. He has authored more than 20 scientific articles and one book chapter in the last decade.

IÑAKI ORUE received the Ph.D. degree from the Universidad del País Vasco (UPV–EHU), in 1989.

He is currently working as a General Facilities Technician with the Science Faculty Division, UPV–EHU. He has authored more than 100 scientific articles that have deserved near 2000 citations.

ANA GARCÍA-PRIETO received the Ph.D. degree from the Universidad del País Vasco (UPV–EHU), in 2003.

She is currently working as an Assistant Professor with the Department of Applied Physics, UPV–EHU. She has led three scientific projects in the last ten years. She has been cited more than 600 times. Her research interests include structural and magnetic characterization of magnetic nanostructures, by using synchrotron radiation, and their use for biomedical applications.

ALICIA MUELA is currently a Senior Professor with the Department of Immunology, Microbiology and Parasitology, Universidad del País Vasco (UPV–EHU). She has led more than three scientific projects in the last ten years. She has been cited more than 1000 times.

MARÍA LUISA FERNÁNDEZ-GUBIEDA is currently a Senior Professor with the Department of Electricity and Electronics, Universidad del País Vasco (UPV–EHU). She has led more than 20 scientific projects and authored more than 150 scientific articles that have attracted near 2000 citations.

JAVIER ALONSO is currently an Assistant Professor with the Department of Earth Science and Condensed Matter Physics, Universidad de Cantabria (UC). He is also leading a project on Remotely Controlled Magnetotactic Bacteria for Biomedical Applications. He has published more than 65 scientific articles. He has been cited more than 2000 times.

LUIS FERNÁNDEZ BARQUÍN (Member, IEEE) is currently a Senior Professor with the Department of Earth Science and Condensed Matter Physics, Universidad de Cantabria (UC). He has led more than ten scientific projects in the last ten years. He has been cited more than 2000 times.